IOP Publishing Journal of Physics D: Applied Physics
J. Phys. D: Appl. Phys. **49** (2016) 015302 (6pp) doi:10.1088/0022-3727/49/1/015302

Enhancement of minority carrier lifetimes in n- and p-type silicon wafers using silver nanoparticle layers

Eshwar Thouti[1], Sanjai Kumar[2] and Vamsi K Komarala[1]

[1] Centre for Energy Studies, Indian Institute of Technology Delhi, New Delhi 110016, India
[2] Central Electronics Limited, Sahibabad, New Delhi 201010, India

E-mail: vamsi@ces.iitd.ac.in and eshwariitd@gmail.com

Received 26 August 2015, revised 1 October 2015
Accepted for publication 5 October 2015
Published 18 November 2015

Abstract

The quasi-steady state photo conductance technique is employed to probe effective minority carrier lifetime (τ_{eff}) modifications after integrating silver nanoparticles (Ag NPs) on n-type and p-type silicon wafers with a native oxide surface. Our observations reveal that τ_{eff} modification is very sensitive to Ag NPs size, surface coverage and also wafer type. With an optimized Ag NPs, τ_{eff} is enhanced from 4.4 μs to 10 μs for a p-type silicon wafer, and from 8.1 μs to 14 μs for an n-type silicon wafer. We attributed the enhancement in τ_{eff} to the partial field effect passivation of the silicon surface by the surface plasmon resonance near-fields of Ag NPs after excitation. Our investigations demonstrate that an optimized Ag NPs on any silicon wafer with a native oxide layer can work as both a light trapping and a surface-passivating layer.

Keywords: minority carrier lifetimes, silver nanoparticles, field effect passivation, quasi-steady state photo conductance, Kelvin probe force microscopy

(Some figures may appear in colour only in the online journal)

1. Introduction

It has been the persistent quest of the scientific community to confine light efficiently within silicon solar cells for maximizing power-generating electrons. A branch of plasmonics from nanophotonics is a fast emerging research area to alter the fundamental physical processes in materials, as well as in devices. One of these processes is light confinement for enhancing optical absorption in various opto-electronic devices using sub-wavelength metal nanostructures [1–5]. Apart from optical confinement, other important electronic properties like minority carrier lifetimes, carrier diffusion lengths and charge carrier mobilities modification in silicon-based opto-electronic devices by metal nanostructures still need to be explored systematically. There are a few hypotheses [5–7], but there is no direct evidence for how carrier lifetimes bring about modifications after the integration of metal nanoparticles (NPs) on silicon wafers and silicon-based solar cells.

A few reports recently demonstrated that when metal NPs are in direct contact with a silicon solar cell, the interface acts as a charge carrier recombination region [5–7]. Usually, the recombination rate depends on the minority carrier lifetime. As a result, estimation of the photo-generated charge carrier lifetime is one of the most useful tools since it directly relates to the diffusion length of charge carriers regardless of the carriers' mobility. The carrier lifetime not only influences the photocurrent but also the photovoltage of a solar cell, which is very sensitive to recombination in light absorbing cell material. The minority carrier lifetime should have an optimum value for reaching reliable solar energy conversion efficiency in a sustainable way using silicon solar cells.

Here, we investigated the effective minority carrier lifetime (τ_{eff}) of silicon wafers after integrating a Ag NPs layer using the quasi-steady state photo conductance technique. We observed that Ag NPs of various size and surface coverage which have integrated on the silicon wafer work as a partial field effect passivation layer. Kelvin probe force microscopy

(KPFM) is used for estimating the work function of Ag NPs to explain our experimental findings with band alignment at the Ag NPs/silicon interface.

2. Experimental methods

One side polished p-type and n-type silicon wafers with a (1 0 0) orientation, a diameter of 2″, a thickness of ~250 μm and a resistivity of ~1 Ω cm were used for this study. Before Ag NPs preparation, all silicon wafers were cleaned by the normal cleaning procedure (ultrasonic cleaning in DI water, propanol and finally with acetone for 10 min in each solution), and then dried with a nitrogen (N_2) jet. In all silicon wafers, a native oxide layer is present. All the bare silicon wafers were pre-annealed at 300 °C in N_2 ambient to avoid temperature-dependent modifications in the τ_{eff}. Silver NPs were prepared on silicon wafers from thermally evaporated discontinuous Ag films with a mass thickness of ~ 5, ~10 and ~15 nm, and were then annealed at 300 °C in ambient N_2 for 1 h. For simplicity, the samples are named with and without Ag NPs as p_Si_5, p_Si_10, p_Si_15 and p_Si_0 related to the p-type wafers, and n_Si_5, n_Si_10, n_Si_15 and n_Si_0 related to n-type wafers; the numbers represent the Ag film mass thickness. Silver NPs were also prepared on glass substrates for work function estimation; special arrangements were made for providing a conducting path on these samples.

The total reflectance (TR) spectra of samples were recorded using a Perkin Elmer Lambda 1050 UV–Vis–NIR spectrophotometer with a 150 mm integrating sphere as an attachment. The τ_{eff} values were estimated using the microwave-detected photo conductance of the carriers; for this purpose we employed a Sinton WCT-120 lifetime tester in quasi-steady state mode (QSSPC). It consists of a flash lamp for generating a white and infrared light spectrum with an intensity of ~50 suns (1 sun = 100 mW cm^{-2}). The tapping mode of an atomic force microscope (AFM, Bruker) was used for recording the surface morphology of the Ag NPs. The surface contact potential difference (CPD) measurements were carried out using Kelvin probe force microscopy (Bruker Instruments), which was used in amplitude modulation mode (AM-KPFM). All measurements were conducted at room temperature and in ambient conditions.

3. Results and discussion

Figure 1 shows the scanned AFM images of Ag NPs formation related to samples p_Si_5, p_Si_10 and p_Si_15. An increase in Ag film thickness from ~5 nm to ~15 nm led to an increase in NP size with a reduced surface coverage. The estimated average NP sizes were ~75 nm, ~150 nm and >200 nm for samples p_Si_5, p_Si_10 and p_Si_15, respectively. Digital photographs of the Ag NPs-integrated silicon wafers are also shown as insets in figure 1, which clearly demonstrate that light interaction is modified by the presence of Ag NPs of various size and concentration with the manifestation of different colours. The appearance of a silicon wafer of a light blue colour (inset of figure 1(a)) with ~75 nm Ag NPs (p_Si_5) is due to an increased TR at the dipolar surface plasmon resonance (SPR) region, and a slightly reduced TR in the long wavelength region. With an increase of Ag film thickness to ~10 nm, the wafer looks pale yellowish in colour (inset of figure 1(b)), which is due to a red shift in the TR maximum and slightly reduced TR in the long wavelength ($\lambda > 800$ nm) region (figure 2). A reddish-grey colour with larger NPs (sample p_Si_15) is due to an increased TR in the long wavelength ($\lambda > 600$ nm) region, with a reduced reflection from the blue region (figure 2).

The total reflectance spectra of silicon wafers with and without Ag NPs are presented in figure 2. The reflectance is very sensitive to the initial Ag film thickness as compared to sample p_Si_0 due to the formation of NPs of various size and surface coverage. With an increase in Ag film thickness, an increase of TR is observed near the dipolar SPR region as well as red shifts in the SPR peak positions of the Ag NPs. At the off-resonant SPR region (~750 nm to 1200 nm), a slightly reduced TR from sample p_Si_10 is observed, which is due to the interacting SPRs of optimum size and concentration of Ag NPs [8, 9]. In the sample p_Si_15, an increased TR is observed after wavelengths of 600 nm due to the out-coupling of light, which is also an indication of the transition from smaller to larger NP formation. For wavelengths smaller than the dipolar SPR region, a reduced TR (valley) can be seen for samples p_Si_10 and p_Si_15 due to the quadrupolar SPR from the relatively larger NPs, which predominantly scatter in a forward direction [4, 9].

From the 320 to 1200 nm spectral region, the reduced TR from samples p_Si_5 and p_Si_10 is ~1.7% and ~3.2%, respectively, and the increased TR from sample p_Si_15 is ~2.6%. The increased/decreased reflectance of incident light from silicon wafers is moderate after the integration of the Ag NPs. Moreover, optical losses in Ag NPs, i.e. interband transitions and Ohmic/parasitic absorption losses appear at short wavelengths, which can suppress light transmission into the silicon despite the reduced TR [10]. Figure 3 shows the absorptance (A), total transmittance (TT) and TR spectra of Ag NPs prepared from (a) ~5 nm Ag thin film, and (b) ~10 nm Ag thin film on glass substrates. Absorptance spectra are calculated using the relation $A = 100\text{-TT-TR}$, where the TT and TR spectra are experimentally measured. From these observations, it is apparent that Ohmic losses are strong near the dipolar and quadrupolar SPRs region, and also broadened upon an increase in NP size (sample p_Si_10). Interpreting TR spectra without considering the Ohmic losses in Ag NPs may be misleading. Therefore, part of the decreased TR at the quadrupolar SPR could be due to Ohmic losses. Due to these parasitic absorption losses, light trapping after the integration of Ag NPs must only be considered for wavelengths larger than the dipolar SPR region. Hence the small reduced reflectance for samples p_Si_5 and p_Si_10 is ~1.9% (for $\lambda > 535$ nm) and ~3.6% (for $\lambda > 780$ nm), respectively, and can be balanced by increased reflectance near the dipolar SPR region and self-absorption losses in the Ag NPs. We will try to relate these optical observations to variation in the τ_{eff} values in the latter part of the discussion. The morphological and spectral features of Ag NPs prepared on n-type silicon wafers

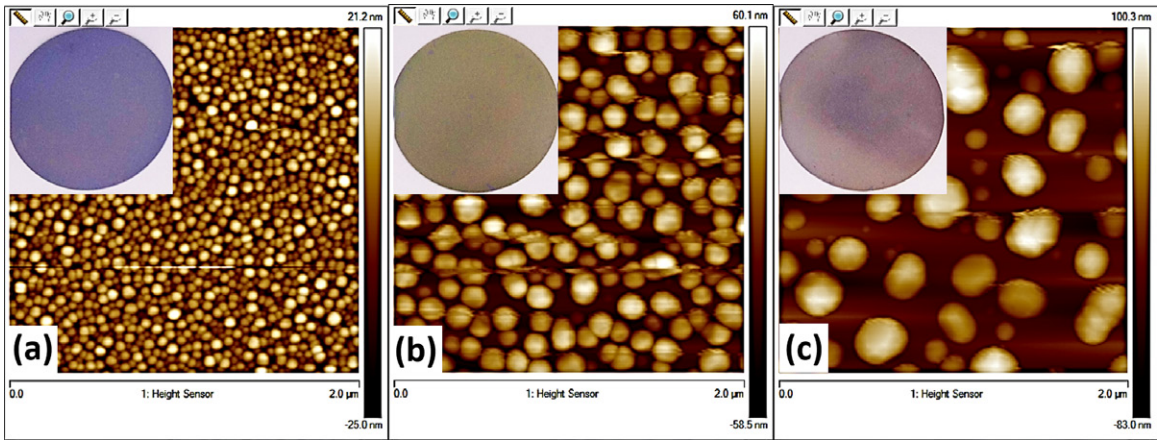

Figure 1. AFM images of silver nanoparticles prepared on p-type silicon wafers from silver thin films of; (a) ~5 nm, (b) ~10 nm and (c) ~15 nm after annealing at 300 °C. Insets of figures show digital photographs of the corresponding wafer samples.

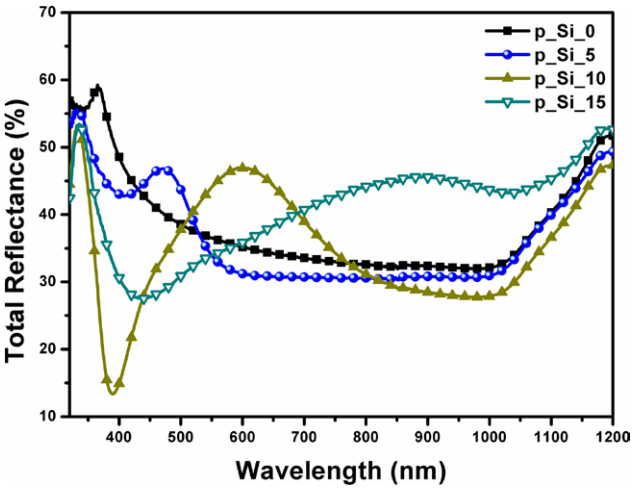

Figure 2. Total reflectance spectra of a silicon p-type wafer with and without silver nanoparticles prepared from films with a thickness of ~5 nm, ~10 nm and ~15 nm after annealing at 300 °C.

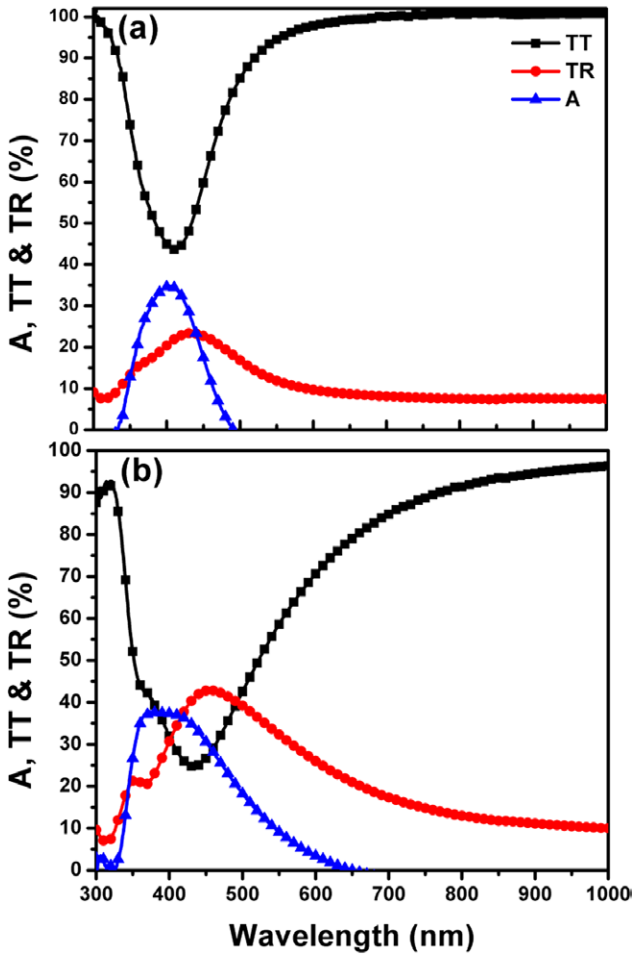

Figure 3. Absorptance (A), total transmittance (TT) and total reflectance spectra (TR) of Ag nanoparticles prepared with (a) ~5 nm, and (b) ~10 nm Ag thin film on glass substrates after annealing at 300 °C.

are also nearly similar. Hence micrographs and the TR spectra of these samples are not presented here.

Figure 4 shows an excess carrier density-dependent τ_{eff} of p-type and n-type silicon wafers with and without Ag NPs. The τ_{eff} values are compared at an excess carrier density of ~5 × 10^{14} cm^{-3}, and the corresponding lifetime values are also summarized in table 1. With the increase in light intensity, τ_{eff} values are increased due to initially saturated Shockley–Read–Hall recombination sites, which become inactive with excess carrier generation [11]. The τ_{eff} values are enhanced after the integration of Ag NPs, and an important observation is the sensitivity of the τ_{eff} values with the size and coverage of the Ag NPs on both types of wafers. Silicon wafers (both n- and p-types) which integrated with Ag NPs of a small size (~75 nm) and large concentration exhibited an enhancement of τ_{eff} values for sample p_Si_5 from 4.4 to 8.2 μs, and for sample n_Si_5 from 8 to 11.1 μs. With relatively larger Ag NPs (~150 nm) and a slightly reduced concentration, sample p_Si_10 exhibited maximum enhancement of τ_{eff} from 4.4 to 10 μs, and sample n_Si_10 from 8.1 to 14 μs. On the other hand, when the size of the Ag NPs is >200 nm, the τ_{eff} is almost unmodified in the case of the p_Si_15 sample, whilst a small enhancement is observed for sample n_Si_15 (from 8 to 9.5 μs). The maximum enhancement in τ_{eff} is observed with Ag NPs of ~150 nm and with moderate surface coverage on both the wafers. Here, we would like to mention that with each flash of light, a simultaneous excitation of the SPRs of

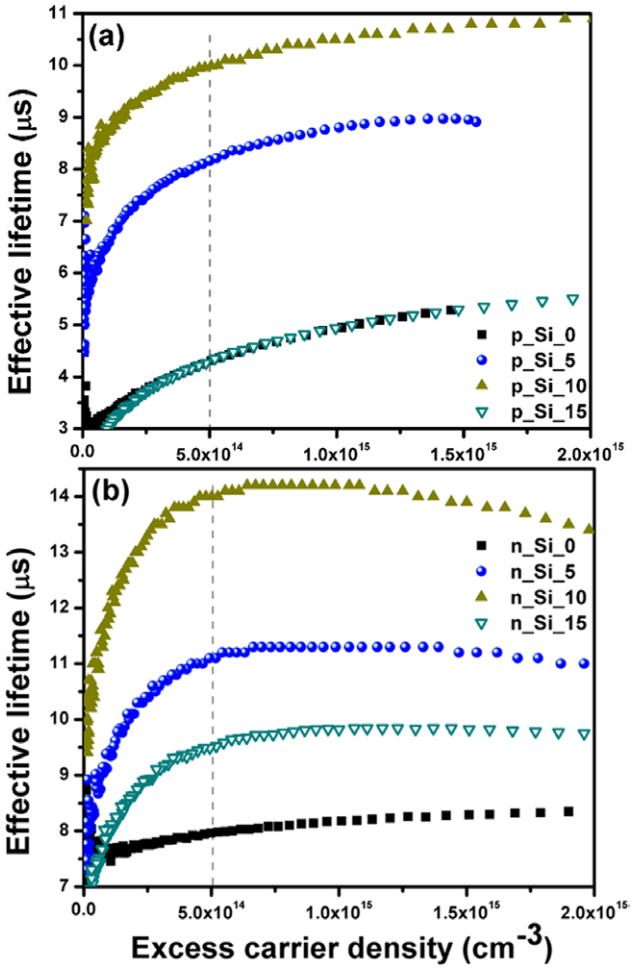

Figure 4. Excess carrier density-dependent effective minority carrier lifetimes of silicon wafers without (p_Si_0 or n_Si_0) and with silver nanoparticles prepared from silver thin films of ~5, ~10 and ~15 nm after annealing at 300 °C on (a) p-type, and on (b) n-type silicon wafers.

Ag NPs and the photo-carriers in silicon wafers is expected due to a wide spectral range of illumination.

The τ_{eff} is affected by the bulk carrier lifetime as well as the surface recombination (SR) velocity [12]. The SR originates from unsatisfied (dangling) bonds at the surface that occur due to the abrupt termination of lattice periodicity. The passivation of these dangling bonds is mostly performed by depositing thin dielectric layers apart from the light trapping, which can also perform field effect passivation (FEP) due to the presence of fixed charges in the thin layers [13]. For the FEP of silicon surfaces to reduce SR, the electric field was also applied externally [14], and ionic charges were introduced to the silicon surfaces [15]. In the FEP process, either of the photo-excited charge carriers is screened away from the surface due to electrostatic fields, meaning that the SR process will be reduced. We also expect some type of FEP with Ag NPs after the excitation of SPR near-fields. The moderately modified reflectance and parasitic absorption in Ag NPs show that active absorption in silicon is not much for photo carrier generation. As a result, we can neglect the bulk carrier lifetime value's effect on the enhanced τ_{eff} values. The modified τ_{eff} is therefore entirely due to variations in the SR process with Ag NPs on the silicon surface.

The variation in SR led to a difference in τ_{eff} with modified Ag NPs sizes and surface coverage, which enables us to think about how silicon wafers support Ag NPs, what proportion of SPR near-fields is coupled or distributed within surface, and also the modified charge quantity on the NP surface during plasmon oscillations. The extension and interaction of near-fields on the surface is different depending on the size, shape (due to contact area variation) and concentration of metal NPs. After producing dipole and quadrupolar oscillators with light, the interaction among them can lead to a change in electric field distribution on the wafer surface based on NP size and concentration. If we look into the optical properties of figures 2 and 3, the variation of absorption and scattering cross sections is due to a variation in the optical near-fields of Ag NPs coupling to silicon. From figure 3, we can see the broadened absorption spectrum of the Ag NPs from sample p_Si_10 compared to sample p_Si_5, which clearly reflects the relatively large near-field generation after absorption from sample p_Si_10. The observed long wavelength reflectance reduction (>800 nm) from sample p_Si_10 is due to the interacting near-fields of optimized Ag NPs sizes through the waveguide modes on the substrate due to the optimum distances [9, 16]. The interacting near-fields of Ag NPs thus distribute uniformly on the silicon surface in order to screen the generated charge carriers effectively in sample p_Si_10 and reduce SR. The observed maximum enhancement of τ_{eff} from samples p_Si_10 and n_Si_10 supports the above arguments that concentrated near-fields seem to be optimum after absorption and also interaction of the metal NPs of the SPRs to the wafer surface. The smaller Ag NPs (samples n_Si_5 and p_Si_5) led to little τ_{eff} enhancement due to their inability to convert optical energy into near-fields and further couple effectively to the waveguide modes at the interface despite the small distances, which can also be seen from the TR spectrum. The large Ag NPs (samples n_Si_15 and p_Si_15) showed very little or no enhancement in τ_{eff} values—the 2D NP layer acting as a random back scatter instead of an anti-reflection layer—from which we can infer that optical energy is not converted into sub-wavelength near-fields after interaction for SR modification. From these observations, we can infer that the characteristic decay length of SPR near-field profile variations into substrate, and the interaction between them influences the SR rate on the surface.

To understand the proposed FEP by Ag NPs on the silicon surface, a schematic of electronic band alignment between silicon and Ag NPs is crucial. For this purpose, the CPD of all samples was measured, and these values were further used for calculating the work functions of samples using the relation $qV_{CPD} = \Phi_{tip} - \Phi_{sample}$ [17]. The estimated mean work function (Φ) values of n-silicon and p-silicon wafers are found to be ~4.18 and ~4.72 eV, respectively. Furthermore, the Ag NPs size-dependant Φ was found to be ~5.12, ~4.97 and ~4.71 eV for ~5 nm, ~10 nm and ~15 nm Ag films, respectively. Similar to our observations, the size-dependant work function for metal NPs has also been reported in the literature [18]. The electron affinity of native oxide is considered

Table 1. Effective minority carrier lifetimes of bare- and silver-nanoparticle-integrated p-type and n-type silicon wafers; ~5, ~10 and ~15 represent the silver film thicknesses in nanometers.

	Effective carrier lifetimes (μs)					
Silicon wafers	p_Si_5	p_Si_10	p_Si_15	n_Si_5	n_Si_10	n_Si_15
Without nanoparticles	4.4	4.4	4.3	8	8.1	8
With Ag nanoparticles	8.2	10	4.3	11.1	14	9.5

Note: Lifetime values are compared at the excess carrier density of ~5 $\times$ 10^{14} cm^{-3} after excitation.

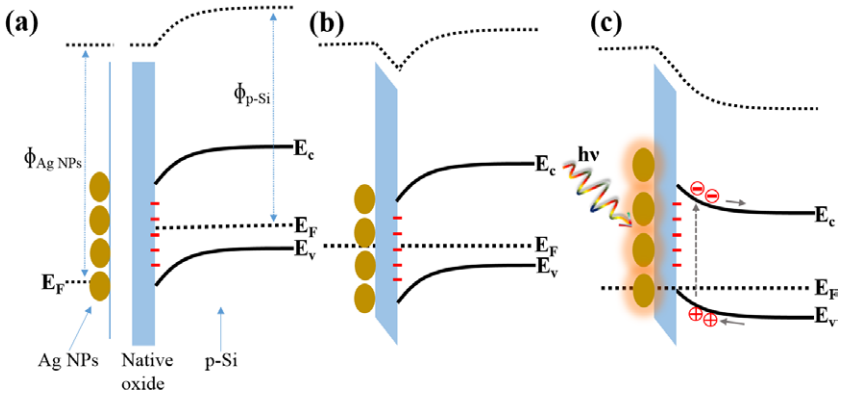

Figure 5. Schematic of energy band alignment at the interface between silver nanoparticles and p-type silicon wafers with a native oxide layer; (a) before contact, (b) after contact without illumination, and (c) after contact with illumination.

to be ~0.9 eV from reference [19]. The schematic describing energy band alignment among p-type silicon, native oxide and Ag NPs is illustrated in figure 5. Here, the energy scale is not normalized to the length scale. Figure 5(a) shows the energy band diagram of Ag NPs and p-type silicon wafers with a native oxide before physical contact. At the Si-SiO_2 interface, downward-band-bending is expected on the silicon side due to a large number of interfacial states, and these states promote the surface recombination of photo- generated charge carriers. After physical contact (figure 5(b)), the Fermi levels in Ag NPs and p-type silicon line up at thermal equilibrium. No further band bending is expected on the silicon side of the Si/SiO_2 interface—instead there will be a potential drop across the SiO_2 [19]. When this structure is illuminated with a flashlight (figure 5(c)), SPR near-fields around the Ag NPs and photoelectrons in silicon wafers will be generated. The oscillating electric fields of the flashlight can generate SPRs of Ag NPs in the visible frequency range. These oscillating dipoles/quadrupoles of Ag NPs and their interaction on the SiO_2 (SiO_2 can hold oscillating electrons better than air due to its large dielectric constant) side can turn into a negatively charged surface; consequently the bands bend upward and the interface acts as an accumulation region at the SiO_2/Si interface. This phenomenon is something which is common in charge-coupled devices, where the negative charge on one side of the SiO_2 creates an accumulation on the other side of it, which can lead to reduced surface recombination [19]. The unavailability of electrons at the interface can reduce the SR; thus the Ag NPs 2D layer works as a partial FEP. The large enhancement in τ_{eff} clearly shows that the confined near-fields around NPs demonstrate good passivation performance. Such phenomena can also be expected in n-type silicon wafers in the τ_{eff} values modification.

Recently, the conversion of optical power directly into positive/negative electrical potentials using metal NPs with supporting conducting structures was demonstrated [20]. Therefore, the observed charge carrier screening phenomena at the interface for the modification of SR need further investigation in order to quantify the near-field potentials and polarity of various sizes, shapes and concentrations of metal NPs, as well as the supporting structures' (SiO_2 or Si) role with incident polychromatic/monochromatic light spectra of different intensities. After integrating Ag NPs, which have had the native oxide (SiO_2) removed from the surface using the RCA cleaning procedure, the reduced carrier lifetime of silicon wafers is due to an increase in the SR process with the generation of recombination centres at the interface [21]. It seems that the native SiO_2 layer can reduce the SR velocity by providing electronic isolation between the silicon and Ag NPs. It seems that optimized very thin dielectric spacer layers will support the optical near-fields effectively with high-driving field intensity through SiO_2 into silicon for a better FEP due to the graded refractive index medium between metal NPs and silicon [22].

4. Conclusions

Silver NPs of various size and surface coverage were integrated on n- and p-type silicon wafers for investigating the modification of τ_{eff} values. Irrespective of the Ag NPs size, concentration and wafer type, the τ_{eff} values of the silicon wafers were enhanced. We found that field effect passivation by the SPR near-fields of Ag NPs at the interface influenced the surface recombination process, which led to enhanced τ_{eff} values. This approach looks to be a potential way of reducing/influencing SR in a controlled and durable manner

for surface passivation, along with light trapping in weakly absorbing silicon material by achieving enhanced lifetimes. The engineering of electromagnetic fields using metal NPs at sub-wavelengths for altering carrier lifetimes with surface passivation has great potential for any opto-electronic device.

Acknowledgments

The authors acknowledge the Nanoscale Research Facility of the Indian Institute of Technology, Delhi for the AFM, KPFM and optical measurements of all samples.

References

[1] Hylton N P *et al* 2013 Loss mitigation in plasmonic solar cells: aluminium nanoparticles for broadband photocurrent enhancement in GaAs photodiodes *Sci. Rep.* **3** 2874
[2] Atwater H A and Polman A 2010 Plasmonics for improved photovoltaic devices *Nat. Mater.* **9** 205
[3] Zhang Y, Stokes N, Jia B, Fan S and Gu M 2014 Towards ultra-thin plasmonic silicon wafer solar cells with minimized efficiency loss *Sci. Rep.* **4** 4939
[4] Temple T L, Mahanama G D K, Reehal H S and Bagnall D M 2009 Influence of localized surface plasmon excitation in silver nanoparticles on the performance of silicon solar cells *Sol. Energy Mater. Sol. Cells* **93** 1978
[5] Thouti E, Sharma A K, Sardana S K and Komarala V K 2014 Internal quantum efficiency analysis of plasmonic textured silicon solar cells: surface plasmon resonance and off-resonance effects *J. Phys. D: Appl. Phys.* **47** 425101
[6] Tong C, Yun J, Song H, Gan Q and Anderson W A 2014 Plasmonic-enhanced Si Schottky barrier solar cells *Sol. Energy Mater. Sol. Cells* **120** 591
[7] Yang Y, Pillai S, Mehrvarz H, Kampwerth H, Ho-Baillie A and Green M A 2012 Enhanced light trapping for high efficiency crystalline solar cells by the application of rear surface plasmons *Sol. Energy Mater. Sol. Cells* **101** 217
[8] Nakayama K, Tanabe K and Atwater H A 2008 Plasmonic nanoparticle enhanced light absorption in GaAs solar cells *Appl. Phys. Lett.* **93** 121904
[9] Thouti E, Chander N, Dutta V and Komarala V K 2013 Optical properties of Ag nanoparticle layers deposited on silicon substrates *J. Opt.* **15** 035005
[10] Spinelli P and Polman A 2012 Prospects of near-field plasmonic absorption enhancement in semiconductor materials using embedded Ag nanoparticles *Opt. Express* **20** A641
[11] Brendel R 2011 *Thin Film Crystalline Silicon Solar Cells: Physics and Technology* (New York: Wiley)
[12] Rein S 2004 *Lifetime Spectroscopy: a Method of Defect Characterization in Silicon for Photovoltaic Applications* (New York: Springer)
[13] Aberle A G 2000 Surface passivation of crystalline silicon solar cells: a review *Prog. Photovolt: Res. Appl.* **8** 473
[14] Ichimura M, Hirano M, Tada A, Arai E, Takamatsu H and Sumie S 2000 Characterization of Si wafers by μ-PCD with surface electric field *Mater. Sci. Eng.* B **73** 230
[15] Bonilla R S and Wilshaw P R 2014 A technique for field effect surface passivation for silicon solar cells *Appl. Phys. Lett.* **104** 232903
[16] Stuart H R and Hall D G 1998 Enhanced dipole-dipole interaction between elementary radiators near a surface *Phys. Rev. Lett.* **80** 5663
[17] Melitz W, Shen J, Kummel A C and Lee S 2011 Kelvin probe force microscopy and its application *Surf. Sci. Rep.* **66** 1
[18] Schnippering M, Carrara M, Foelske A, Kotz R and Fermin D J 2007 Electronic properties of Ag nanoparticle arrays. A Kelvin probe and high resolution XPS study *Phys. Chem. Chem. Phys.* **9** 725
[19] Janesick J R 2001 *Scientific Charge-Coupled Devices* vol PM83 (Bellingham, WA: SPIE) p 244
[20] Sheldon M T, Van de Groep J, Brown A M, Polman A and Atwater H A 2014 Plasmoelectric potentials in metal nanostructures *Science* **346** 828
[21] Zaghouani R B, Manai L, Rezgui B D and Bessais B 2015 Study of silver nanoparticles electroless growth and their impact on silicon properties *Chem. J.* **1** 90
[22] Powell A W, Wincott M B, Assender H E and Smith J M 2013 Controlling the optical scattering of plasmonic nanoparticles using a thin dielectric layer *J. Appl. Phys.* **113** 184311